*Work partially supported by U. S. Air Force Cambridge Research Laboratories Contract No. F19628-71-C-0060 through Emmanuel College.

[1]H. J. Bhabha, Proc. R. Soc. Lond. A152, 559 (1935).
[2]G. Racah, Nuovo Cimento 14, 93 (1937).
[3]M. M. Block, D. T. King, and W. M. Wada, Phys. Rev. 96, 1627 (1954).
[4]T. Murota, A. Ueda, and H. Tanaka, Prog. Theor. Phys. 16, 482 (1956).
[5]B. P. Roe and S. Ozaki, Phys. Rev. 116, 1022 (1959); J. F. Gaebler, W. E. Hazen, and A. Z. Hendel, Nuovo Cimento 19, 265 (1961). P. H. Stoker, C. Hofmeyr, and C. H. Bornman, Proc. Phys. Soc. Lond. 78, 650 (1961); P. D. Kearny and W. E. Hazen, Phys. Rev. 138, B173 (1965).
[6]R. L. Kinzer and J. R. Burwell, Phys. Rev. Lett. 20, 1050 (1968).
[7]H. Crane and J. Halpern, Phys. Rev. 55, 838 (1938).
[8]F. J. Loeffler, Phys. Rev. 108, 1058 (1957).
[9]M. Gailloud and C. Piron, Helv. Phys. Acta 36, 164 (1963).
[10]S. L. Leonard, Bull. Am. Phys. Soc. 111, 167 (1956). The point in Fig. 2 is based on the value quoted by Loeffler (Ref. 8).
[11]M. Koshiba and M. F. Kaplon, Phys. Rev. 100, 328 (1955).
[12]J. E. Naugle and P. S. Freier, Phys. Rev. 104, 804 (1956).
[13]V. A. Tumanyan, G. S. Stolyarova, and A. P. Mishakova, Zh. Eksp. Teor. Fiz. 37, 355 (1959) [Sov. Phys.—JETP 37, 253 (1960)].
[14]A. S. Cary, W. H. Barkas, and E. L. Hart, Phys. Rev. D 4, 27 (1971).
[15]J. Böhm, A. Matlova, J. Zacek, and V. G. Grishin, Nucl. Phys. B32, 632 (1971).
[16]M. Camac, Phys. Rev. 88, 745 (1952).
[17]L. Criegee, Z. Phys. 158, 433 (1960).
[18]B. Grossetête, R. Tchapoutian, D. J. Drickey, and D. Yount, Phys. Rev. 168, 1475 (1968).
[19]S. C. Frautschi, Suppl. Prog. Theor. Phys. 8, 21 (1958).
[20]C. Piron, M. Gailloud, Ph. Rosselet, and M. Biasutti, Helv. Phys. Acta 33, 945 (1960).
[21]M. Koshiba and M. F. Kaplon, Phys. Rev. 97, 193 (1955).

PHYSICAL REVIEW D VOLUME 9, NUMBER 3 1 FEBRUARY 1974

Measurements of the differential cross section of the reaction $pp \to d\pi^+$ from 3.0 to 5.0 GeV/c*

H. L. Anderson, D. A. Larson,† and L. C. Myrianthopoulos
The Enrico Fermi Institute, The University of Chicago, Chicago, Illinois 60637

L. Dubal,‡ C. K. Hargrove, E. P. Hincks,§ R. J. McKee, and H. Mes||
The National Research Council of Canada, Ottawa, Canada K1A OR6

D. Kessler and A. C. Thompson**
Carleton University, Ottawa, Canada K1S 5B6

(Received 28 August 1973)

A measurement of the complete differential cross section for the reaction $pp \to d\pi^+$ at 3.00, 3.20, 3.43, 3.65, 3.83, 4.00, 4.20, and 5.05 GeV/c incident proton momentum has been made in an attempt to establish the role of the $\Delta(1950)$ in this region. The data show that the previously observed enhancement in the forward cross section between 3 and 4 GeV/c due to this isobar is an effect which damps out quickly as the production angle departs from zero degrees, in contrast with the well-known enhancement at 1.35 GeV/c, which is evident at all angles. In particular, the one-pion-exchange model is in poor agreement with the extended set of data. A detailed description is given of a novel proportional-wire-chamber system which facilitated the selection of this rather rare reaction from a very high competing background.

I. INTRODUCTION

This is a report on a comprehensive series of measurements of the complete angular distribution and total cross section for the reaction

$$pp \to d\pi^+ \qquad (1)$$

over the range of incident momenta from 3.00 to 5.05 GeV/c. These measurements were carried out at the Bevatron of the Lawrence Berkeley Laboratory as an extension of previous work of our collaboration on reaction (1).[1]

The low-energy region,[2] below 2.3 GeV/c for reaction (1), has been successfully described in terms of the excitation of the (3, 3) resonance.[3] Between 2.3 and 4.3 GeV/c the forward cross section shows another structure which may be ascribed to the (7, 3) resonance.[4-8] The purpose of

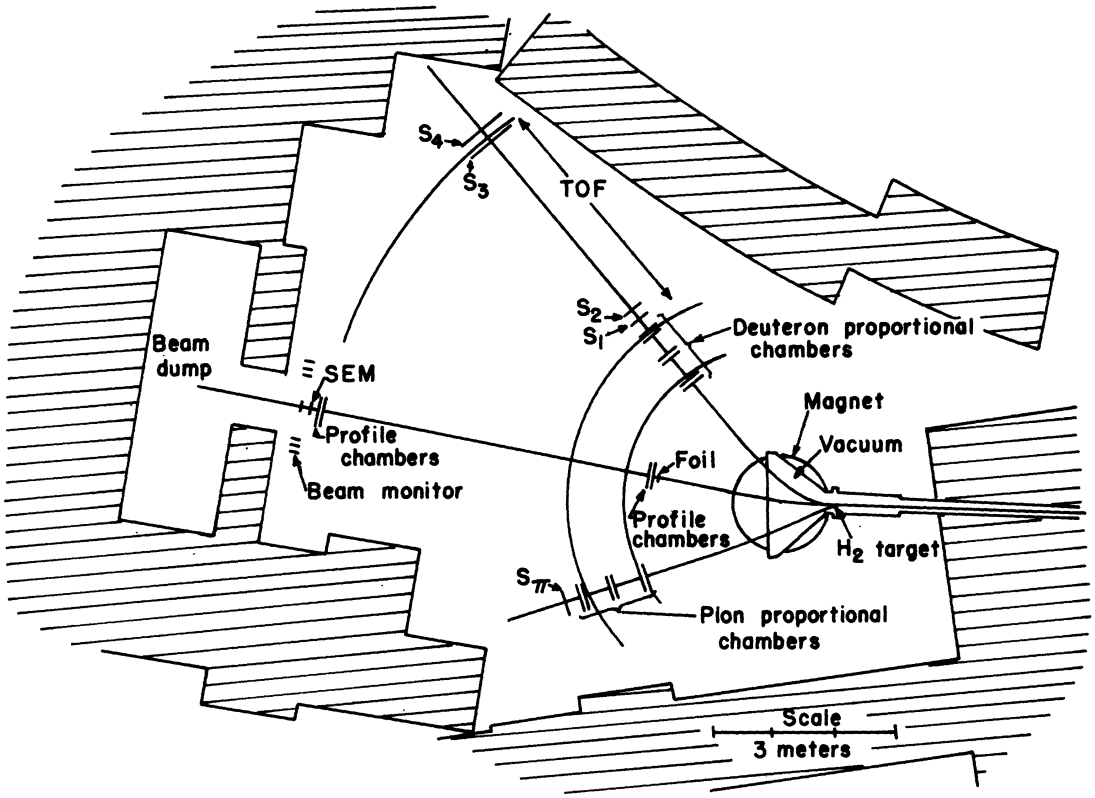

FIG. 1. Plan view of the apparatus.

this experiment was to bring more systematic and more complete data to this region to see to what extent the angular distribution is affected by the $\Delta(1950)$ resonance. Recently, Barry[9] and Sundaresan and Watson[10] have extended the original work of Yao[5] on the one-pion-exchange model, making it possible to compare our data with the theory over the full angular range. The dynamical quantity Δ, used by Kerman and Kisslinger[11] to describe the pickup mechanism, was found to be useful in the analysis of our data as an energy-independent parameter.

The use of event-selecting proportional wire chambers facilitated this experiment. We were able to collect high statistics on a small-cross-section reaction in the presence of much more frequent "background" processes.

II. APPARATUS

The experiment was designed to cover the complete angular range in the center-of-momentum (c.m.) system. However, due to the identity of the initial-state particles, it was sufficient to measure the final-state c.m. angular distribution over the range 0°–90°, corresponding to forward pions and backward deuterons. Both final-state particles were detected in a two-arm spectrometer using a single large magnet.

The general arrangement is shown in Fig. 1. The deuteron and pion, produced in a small target suspended in a large vacuum tank, passed through a large analyzing magnet and were detected in coincidence in two spectrometer arms. The pion spectrometer arm consisted of six multiwire proportional chambers (three crossed pairs) and a single scintillation-counter array, S_π; the deuteron spectrometer arm also consisted of six proportional chambers and, in addition, a scintillation-counter time-of-flight system (S_1, S_2, S_3, S_4). Beam intensity and beam profile monitors were provided as shown.

The system of fast detectors with low dead time (multiwire proportional chambers and scintillation counters) used the kinematic properties of $pp \to d\pi^+$ to extract these events from the other pp processes. The proportional-chamber system, operating in a decision-making mode, automatically checked the momenta, coplanarity, and opening angle of the particles in the two arms every time a particle appeared in each arm in tight time coincidence. Up to 3×10^5 particles per second in each

arm were digitized by the proportional chambers. When a coincidence occurred the addresses from four pairs of the chambers were compared with precalculated sets of values by digital comparators. As a result, only those events with the kinematically correct relationships were accepted. A PDP-9 computer was used to further test events on line, monitor the operation of the hardware, and do normal bookkeeping. On-line hardware and software cuts, together with off-line software cuts, yielded a very clean separation of reaction (1) from real and accidental background. Cross sections were ultimately extracted from taped data using the Lawrence Berkeley Laboratory CDC-6600 computer.

A. Proton beam and monitors

The momentum of the Bevatron external proton beam was known to about one part in 1000. The intensity of the beam impinging on the liquid hydrogen target in the experimental area was about 10^8–10^9 protons per pulse. This intensity was varied from run to run with adjustable collimators to keep the total detector and electronic dead time from rising much above 20%. This set a limit of $\sim 3\times10^5$ particles per second in the arms. Spill lengths varied from about 0.3 to 1.5 sec; the repetition rate was approximately 10 pulses per minute.

The beam was monitored by two identical scintillation-counter telescopes, which observed the secondaries produced at 90° when the beam struck a 0.16-cm-thick aluminum plate located on the beam line in front of the entrance to the beam dump. The monitor counts were gated off by dead-time signals from all the detectors in the experiment to take proper account of the dead time of the system. These telescopes were calibrated to give the absolute numer of protons in the beam in a two-step process. Throughout the running we checked the monitor count against C^{11} activation induced in a polystyrene sample. In turn, these C^{11} monitors were calibrated in an absolute way by direct counting of the protons traversing them using scintillation counters at a beam intensity reduced below 3×10^6 protons per second. As a by-product of this work we determined the cross section for the production of C^{11} from natural carbon at 4.5 GeV/c to be 27.7 ± 0.3 mb. The details of this measurement will be reported elsewhere.[12]

A polystyrene sample was placed in the beam near the upstream profile monitor. The sample, consisting of a 3.8-cm-diameter disk surrounded by and coaxial with an annulus of 7.6 cm outside diameter, was irradiated for about ten minutes while the beam monitor counts were recorded. The activity of the annulus compared to the disk gave a check on the beam halo, typically a few percent. The C^{11} decay, by the reaction $C^{11} \rightarrow B^{11} + e^+$ (with a 20-min half-life), was measured by placing the disk and annulus separately between copper plates to absorb the positrons and detecting the annihilation γ rays with a NaI crystal of known efficiency.

Four beam profile chambers were used to observe the spatial distribution of particles in the beam, spill by spill. These were 10-cm-by-10-cm proportional chambers with 32 readout wires.[13] Two of these chambers, one horizontal and one vertical, were mounted on an optical bench transverse to the beam line, 211 cm downstream from the center of the analyzing magnet. A second crossed pair was mounted on the moveable cart near the beam dump. At the upstream profile monitors the spot size was usually about 2 cm vertically and 0.75 cm horizontally; this implied an even smaller spot size at the target. The beam divergence was 1.5 mrad horizontally and 5 mr vertically.

Coarse beam tuning was carried out with the use of grid-marked scintillators placed in the beam and viewed by television cameras. One scintillator was located within the vacuum tank just upstream of the target and made an angle of 45° with respect to the beam. This scintillator was raised out of the beam during data taking. A second scintillator was centered on the undeflected beam line just downstream of the magnet. Fine tuning was carried out with the beam profile chambers and was checked with Polaroid film.

In order to check beam purity, a few data runs were taken to measure πp elastic scattering. These data indicated that beam contamination by pions was negligible.

B. Liquid hydrogen target

Two different liquid hydrogen targets were used. The first, constructed of Kapton 0.005 cm thick, was 5.08 cm long and 2.54 cm in diameter, having hemispherical ends with a radius of curvature of 1.27 cm. The second, constructed of 0.010-cm Kapton, was 5.34 cm long and 5.08 cm in diameter. It had hemispherical ends with a 5.08-cm radius of curvature. In both cases the target was wrapped with two layers of a 6.4-μ aluminized Mylar superinsulation. The target was surrounded by a 10.2-cm-diameter-by-11.4-cm-long open-ended cylindrical heat shield constructed of 0.041-cm copper, which in turn was wrapped with two additional layers of 6.4-μ superinsulation.

The entire target assembly was positioned with its symmetry axis on the nominal beam line and was located 89 cm upstream from the center of the

analyzing magnet.

In order to reduce the amount of material near the target, and hence reduce the production of background events from the target region, the target was suspended in a vacuum tank whose window was located beyond the center of the magnet, 107 cm from the target. It was constructed of 0.025-cm-thick Kapton and was large enough so that all detected deuterons and pions as well as the unscattered beam passed through it. Its location made it easy to separate deuterons produced in the window from those produced in the target.

C. Analyzing magnet

Prior to the experiment, the Lawrence Berkeley Laboratory Magnet Test Group carried out an extensive mapping of the magnetic field of the large analyzing magnet. The magnet had 152.4-cm-diameter pole tips with a 30.5-cm gap and was operated at either 8 kG or 16 kG. Throughout the experiment, the magnetic field strength was determined by a small, pneumatically driven flip coil, positioned near the center of the lower pole face and read out on a digital voltmeter calibrated directly in gauss.

D. Spectrometer arms and detectors

In order to measure final-state pions and deuterons over the pion angular range 0°–90° c.m. and to measure pp elastic scattering near 90° c.m. (the latter used for calibration checks with published cross sections) it was necessary to place the detectors in a wide variety of positions. This was done by having the arms move independently on two rails concentric with the center of the analyzing magnet.

Each arm held six 40-cm-by-40-cm multiwire proportional chambers (MWPC) mounted with dowel pins in crossed X and Y pairs on three aluminum support frames. The separation between adjacent pairs of chambers was 50 cm. Each arm contained scintillators in addition to proportional chambers. The acceptance of each arm was usually determined by the third pair of chambers, subtending a solid angle at the target of 14 msr.

Each of the multiwire proportional chambers consisted of a 255-wire readout plane with a 1.6-mm interwire spacing (16 wires per inch), located between two high-voltage wire planes. The distance from the readout plane to either of the high-voltage planes was 4.8 mm. The gas used was the Charpak[14] "magic mixture": 72.0% argon, 23.6% isobutane, 4.0% methylal, and 0.4% Freon 13B1. The total chamber mass, as seen by an incident particle, including wires, gas, and gas seal, was 0.049 (g/cm^2)/chamber. The chambers were operated at about 4200 V on a broad plateau several hundred volts wide. The spatial resolution of the chambers, as determined by fitting straight lines to particle trajectories through three chambers, was 1.6 mm (FWHM), equal to the wire spacing.

In addition to the multiwire proportional chambers, each arm contained scintillation counters. The pion arm contained a single 43-cm-by-43-cm scintillation-counter array, S_π, composed of five vertical strips 8.6 cm wide; these were viewed from above and below by an arrangement of Lucite light guides and RCA 8575 phototubes as described in Ref. 1. Two similar scintillation-counter arrays, S_1 and S_2, were mounted on the deuteron cart behind the last pair of deuteron proportional chambers. These counters, together with two larger scintillator arrays, S_3 and S_4, located 4 m behind the first two, provided a twofold measurement of the deuteron time of flight. The larger counters were 84 cm by 84 cm and consisted of five vertical strips 16.8 cm wide, mounted on a large frame that could be rolled along a guide rail. This rail was concentric with the other rails and was located at a radius of 7.4 m about the center of the analyzing magnet. The total mass in the spectrometer arms, including hydrogen target, air, detectors, etc., was 0.99 g/cm^2 in the pion arm and 3.60 g/cm^2 in the deuteron arm. The momentum resolution of the spectrometer varied between 0.1 and 0.2 GeV/c, depending on the setting.

E. Logic

The scintillation counters S_1, S_2, S_3, S_4, and S_π were divided into vertical strips, giving them hodoscope capabilities in the horizontal plane. For each of the deuteron arm scintillation counters a valid signal, called a GO, was obtained only if exactly one upper (U) and one lower (L) phototube, both viewing the same strip, produced a signal in tight time coincidence (within 8 nsec for S_1 and S_2, and within 12 nsec for S_3 and S_4). If additional tubes fired in a given counter, indicating the passage of more than one particle through the detector, the signal was vetoed for that detector. For the pion scintillation counter, S_π, an acceptable signal was obtained whenever at least one upper tube and one lower tube fired, again in tight time coincidence (within 10 nsec). In this case, however, no limit was placed on the number of tubes that could fire, as long as at least one upper and one lower tube fired. This was to avoid the loss of events due to a single particle interacting in or near the scintillator strip. (Such losses in the deuteron scintillators were automatically taken care of by a correction to the cross section made for nuclear

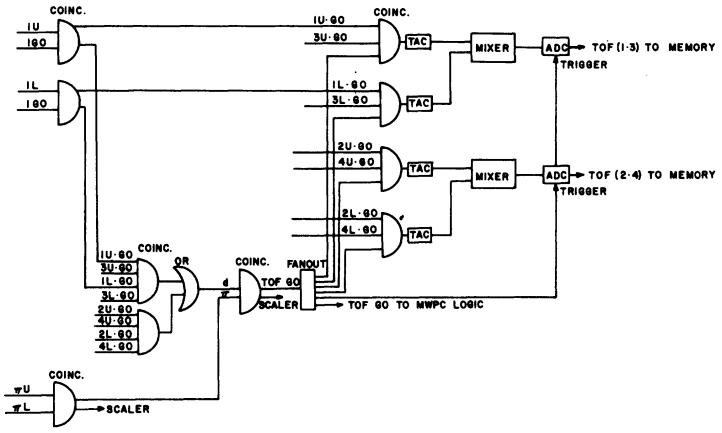

FIG. 2. Block diagram of the TOF logic.

absorption, discussed later.) The logic also provided signals, sent to the computer, identifying those scintillator strips that detected a particle for each event.

To obtain good time resolution in the time of flight (TOF) we used the fact that the sum of the transit times for light from any point in the scintillator to each end is insensitive to position. Since each strip was viewed with two phototubes, one at each end, the spread in time due to vertical position was canceled by measuring the TOF between a pair of counters twice, using the upper tubes for one measurement and the lower tubes for the other measurement, and adding the two. Figure 2 shows a simplified diagram of the scintillation-counter logic that employed this technique. Note that the deuteron time of flight was actually measured twice in this manner. The TOF between S_1 and S_3 uppers was added to that between S_1 and S_3 lowers, thus canceling out the vertical position spread in TOF (1·3). A similar measurement was carried out to obtain TOF (2·4). In each case the digitized TOF signal was sent to the computer, and the final data analysis used the average of the two measurements. Note that the analog-to-digital conversion (ADC) of the TOF signal was carried out only if the signal $S_\pi \cdot (S_1 \cdot S_3 + S_2 \cdot S_4)$ was obtained, where S_π consisted of *at least* one upper and one lower π signal, and where each S_i $(i = 1, 2, 3, 4)$ consisted of *exactly* one upper and one lower signal, both from the same scintillator strip. The TOF resolution obtained was about 1 nsec.

The time required by the logic to digitize the analog TOF signal was less than 12 μsec per event. Only those events were digitized for which a particle appeared in both arms in the scintillators in coincidence (called a TOF GO) and also in coincidence with the proportional chambers.

The encoding of the struck proportional chamber wires into a nine-bit number was carried out by a fast-logic system[15] mounted on the chambers themselves. A typical wire signal, after amplification, set a latch. After a signal set any one latch, further MWPC signals were blocked. The latching time was about 40 nsec per chamber. The latches in each chamber were then tested to see how many had fired. Only single-particle events, defined as events in which one wire or a group of adjacent wires fired, were accepted. The address of the single wire or the average address of the group appeared at the output as a nine-bit word. (The ninth bit was a half-wire bit.) In all other cases, usually implying multiparticle events, the chamber was internally reset.

A novel feature of the experiment was the decision-making mode of operation of the multiwire proportional chambers, which was based on the kinematics of reaction (1). For any given event the coordinates of a deuteron or pion in any one chamber were uniquely correlated with the coordinates in other chambers. Four independent correlations can be tested, corresponding to the four constraints of energy-momentum conservation. These tests involved comparison of horizontal (X) or vertical (Y) coordinates of trajectories, as determined by the proportional chambers, and were equivalent to checking the opening angle, coplanarity, and correlation of angle of emission and particle momentum in each arm. Events which failed one or more of these tests (outside assigned limits, depending on beam spot size, finite target length, multiple scattering, etc.) were rejected. This rejection was carried out in parallel by four hardware comparators.

Figure 3 shows a block diagram of the comparison logic[16] for two chambers whose coordinates were to be compared. During operation each chamber was detecting particles continually, and

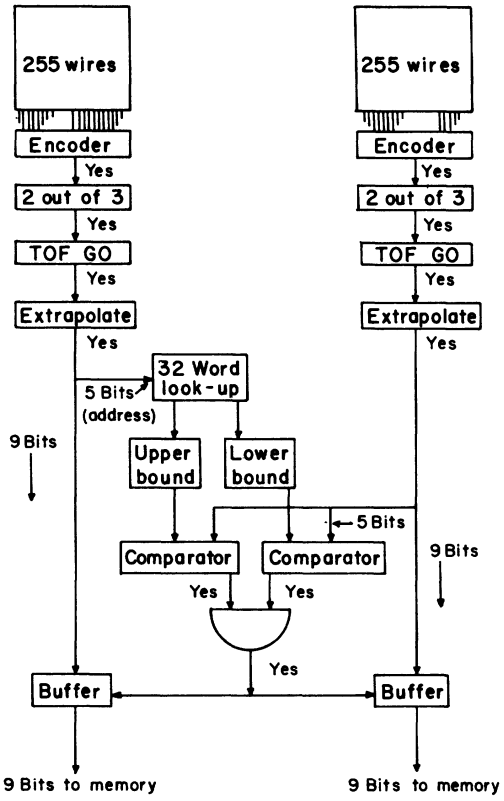

FIG. 3. Block diagram of the comparator logic for two chambers.

the encoder on each was producing nine-bit binary numbers of the struck wires. However, only those chamber coordinates were compared which were produced in coincidence with the TOF GO gate and which also passed the "two out of three" and "extrapolate" logic, discussed later. Only the five most significant bits were used in the comparison. These bits from one chamber were sent as an address to a 32-word look-up table. For each address the look-up table produced an upper bound and a lower bound, which were sent to separate comparator circuits. At the same time, the address from the other chamber was sent to both of the comparators. If this five-bit number was within the limits, the original nine bits from both chambers were sent to memory. Otherwise the event was rejected as being kinematically unacceptable.

Prior to each data run, precomputed upper and lower bounds of the look-up tables were loaded using the computer. During data taking the four hardware comparison tests were run in parallel and required 250 nsec per event.

It has already been mentioned that each of the two spectrometer arms contained three X chambers (X view) and three Y chambers (Y view). Altogether, therefore, there were four sets of three chambers. For each of the four sets of three chambers at least two out of the three chambers were required to fire. This was done to improve the efficiency. However, because only two out of the three were required, it could occasionally happen that a chamber that was to be compared in a hardware comparison test did not fire, and this could cause the hardware comparators to give meaningless results. In this circumstance a hardware extrapolation was made using the other two chambers in the set of three to obtain a five-bit number to be used by the comparators. This hardware extrapolation required 150 nsec. As many as four extrapolations were done in parallel.

In order to monitor the effect of the hardware tests during data taking, scatter plots were displayed on display scopes in which one axis of the scatter plot represented the coordinates of one chamber and the other axis represented the coordinates of the comparison chamber. Events were represented as dots, and the look-up table bounds were displayed as solid lines. A typical coplanarity scatter plot is shown in Fig. 4. Note that the events corresponding to reaction (1) form a narrow band within the center of the look-up table limits.

These hardware tests proved to be very effective. They reduced the quantity of data that otherwise would have been taped by a factor typically 20 and up to 50, depending on the angular position of the detectors, the incident beam intensity, and the bounds of the look-up tables.

It has already been mentioned that the experiment was operated with a dead time of about 20%. Most of this was due to the proportional-chamber logic and only a small fraction to the scintillator logic. At 5×10^5 particles per second incident on the chambers, their dead time was 15%. The dead time per good event was less than 12 μsec and was limited by the time to perform the analog-to-digital conversion of the TOF data.

F. Computer system

Operator control of the experiment during each run, data acquisition and taping, and checks on the equipment were carried out using a PDP-9 computer with a large external memory. The operator initiated and terminated data acceptance, set various hardware and software tests to filter the data, and displayed data as they were accepted in the form of cumulative counts, histograms, and scatter plots on display scopes. A typical run lasted for a few hours, during which a few thousand events were recorded on tape.

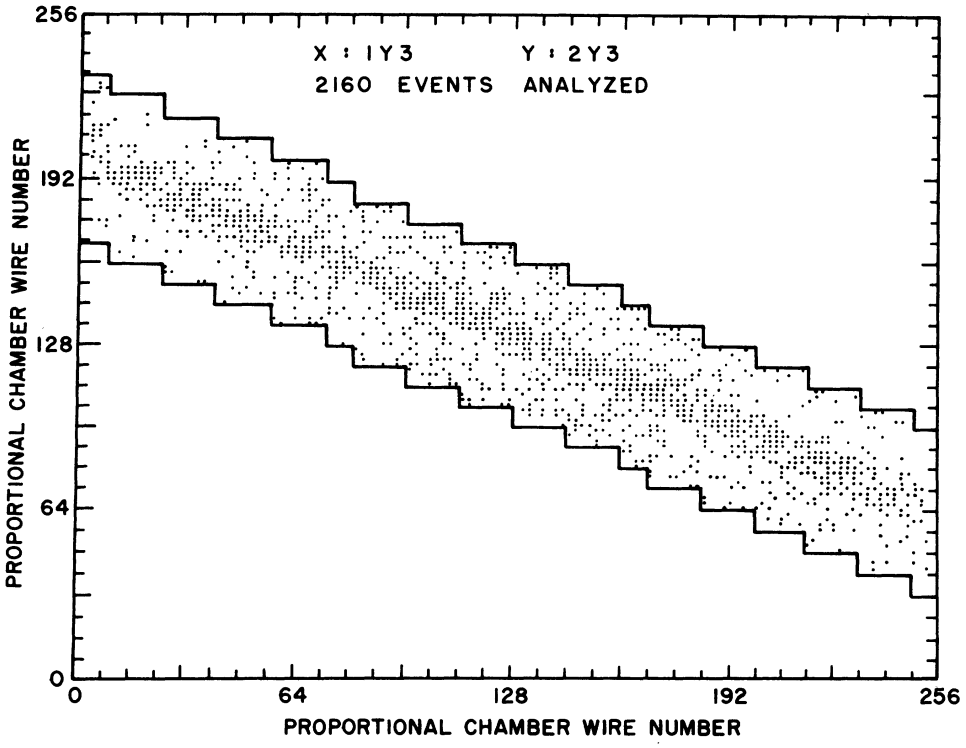

FIG. 4. A typical scatter plot showing the coplanarity correlation between the two spectrometer arms. The third Y chamber of arm one (1Y3) is plotted along the horizontal axis, while the corresponding chamber of arm two (2Y3) is plotted along the vertical axis. The solid lines are the limits set in the hardware comparators.

III. DATA REDUCTION AND ANALYSIS

The data handling can be divided into three distinct parts. This section describes each one in some detail. The first step was data reduction by on-line software. The hardware cuts applied to the data were described in the last section; in addition, the on-line computer that controlled the data collection made further cuts before recording the results onto magnetic tape. The second step was off-line particle retrace and kinematic reconstruction. Cuts on calculated quantities, such as missing masses, were done at that time. The final result from this step essentially consisted of histograms of events in c.m. angle bins and the solid angle for each bin. The third step was to convert these results into differential cross sections using the absolute beam calibration and the various corrections and apparatus efficiencies.

A. On-line analysis

The on-line computer performed continuous checks on the hardware and data. All of these were under operator control by means of commands typed in from a keyboard. Many of the checks were displayed on a storage scope in the form of histograms and scatter plots. One of the most important was the continuous monitoring of the twelve multiwire proportional chambers; wire histograms of each chamber were accumulated and could be inspected at any time. In addition, continuously updated wire-by-wire inefficiency histograms for each chamber were calculated in the computer using the other two chambers of a view as reference.

Data from events that triggered the system and passed the hardware cuts went into the large external memory; they consisted of the twelve wire-chamber coordinates, the two ADC outputs from TOF, and scintillator hodoscope information. At the end of a beam spill the data were read into the computer and processed. In addition, scalers were read into the computer at the end of the spill and reset to zero. The data, consisting of the scaler information (and other "header" information) plus the processed events of that spill, were written as one record on magnetic tape before the next beam spill.

The checks fell into two categories: cuts on individual events and cuts on entire beam spills. One of the checks in the first category was a cut

on track linearity through the chambers. For events which fired all three chambers of a view, it was required that the track be linear to within a preset tolerance, usually three wire spacings; otherwise the event was rejected. The linearity rejection rate was kept by the computer for all four views for later correction to the cross sections. The assumption was that the event was good but that the particle was scattered too much in the chamber for proper kinematic reconstruction. Another check in the first category dealt with the TOF measurements. Since only one out of two TOF's were required in the trigger, the failure rate of each TOF was kept by the computer for a later efficiency correction to the cross sections. Only events which passed the software cuts were recorded on magnetic tape. Secondly, an occasional beam spill was deleted because it did not satisfy reliability criteria as determined by beam monitors, scaler information, or operator decision.

B. Off-line analysis

The off-line processing, which was done on a CDC 6600, took the eight wire coordinates for each event and retraced and reconstructed the event. The ultimate aim in this step of the analysis was to obtain an angular distribution in one-degree bins in the c.m. coordinate system for each run. Using the data themselves in a process described below, the solid angle of each bin was also calculated. Along the way many other kinematic quantities were also calculated and displayed in histograms and scatter plots. Each of these plots could be cut. Thus, a typical data run was analyzed in several passes, the first with no cuts and one or more subsequent passes with cuts. In addition, scaler counts and other "header" information were summed or otherwise processed and printed out along with the distributions.

We first discuss briefly the retrace of pion and deuteron orbits back through the large, inhomogeneous magnetic field. Since it was assumed that the horizontal projection of both types of orbits onto the median plane of the magnet passed through the center of the hydrogen target, an orbit was independently and completely determined by the four wire coordinates of the spectrometer arm that the orbit went through. However, finding the orbit by numerical integration of the equation of motion of the particle through the previously mapped field would have been costly in computer time if done for every event. Therefore, prior to data analysis, a small set of representative orbits for each spectrometer arm was chosen and retraced by numerical integration; with each of these orbits represented by a point in a four-dimensional space (since it took four coordinates to define an orbit), real events were retraced by interpolation in this four-dimensional mesh. By deriving simple sets of transformations between the actual wire-chamber coordinates and the mesh points, the mesh was made rectangular and covered with little waste the physically meaningful orbits; also, the momentum components in the c.m. system at the target were found by simple linear interpolation using the nearest mesh points. With as few as 100 mesh points the interpolation errors were kept to less than 0.5%, negligible compared to the resolution. In addition to the three momentum components, the distance of the orbit above the center of the target (the z position) was also found by the traceback.[17]

With the incident proton momentum known and the final momentum of both pion and deuteron completely determined by the magnetic field, the $pp \to d\pi^+$ reaction was highly overdetermined. Therefore, several kinematic quantities with each distributing itself in a very well defined peak were calculated and displayed in histograms. Some of these quantities were the total momentum component along the beam line in the laboratory frame, the two total momentum components transverse to the beam line, the two missing masses determined by each spectrometer arm alone, and the total missing mass (which should be zero). Since each arm separately and independently determined the c.m. angle of the reaction, θ, and the angle of the reaction plane, ϕ, the differences between the two θ's and ϕ's were also put in histograms. The histogram of $\Delta\theta$, which generally had a width of 3° or 4°, gave an over-all view of the resolution of the spectrometer arms. The mass of the particle through the deuteron arm was directly calculated by using the momentum information from the wire chambers and the two TOF measurements. Finally, both the difference of the two z positions of the orbits and the average z position were calculated. Since each of these histograms revealed different aspects of the data, very generous cuts were applied which usually cleaned up the data very thoroughly. The mass histogram of the particle through the deuteron arm was especially useful in cutting out protons.

A single value for each of θ and ϕ was used in the final analysis for each event. Ideally, in the c.m. frame of reference, the 3-momenta of the pion and deuteron point in exactly opposite directions, but due to effects such as multiple scattering, finite target size, finite wire spacing, etc., the measured 3-vectors were not collinear. Therefore, a weighted average of the vector directions (with the deuteron vector flipped 180° first) was

taken to define θ and ϕ for the event. The reason for using weights was as follows: Recalling that the two tracebacks per event were done to the center of the target, one of the greatest contributions to the resolution of the spectrometer was the finite size of the target. Calculations showed that the c.m. angle resolution was generally different in the two arms due to finite target size. Weights were introduced to reflect this; the weight calculated for a given arm was made inversely proportional to the sensitivity of θ to where the event took place in the target.

Some of the kinematic quantities calculated for histograms were also displayed in two-dimensional scatter plots. A few of these were θ vs ϕ and θ vs the various missing masses. The scatter plots were frequently useful in deciding the size of the kinematic cuts. Occasionally two-dimensional cuts were made on the scatter plots themselves.

The events that survived all the cuts were put into 1° θ bins for the final differential cross-section calculations of the run under analysis. For each bin a histogram in ϕ was collected for the purpose of finding the solid angle in the c.m. system for the bin. Ideally, a ϕ histogram should be a rectangular distribution for bins of zero width in θ and not too near the edge of the spectrometer acceptance. Multiple scattering, finite target size, finite wire spacing, and finite bin width cause the otherwise sharp edges to smear out. As long as the c.m. bin was not too close to the limits of acceptance, the height of the ϕ histogram near its center should have been unaffected. We therefore defined in the central region of each ϕ histogram a fiducial region which was far enough away from the smearing effects of the edges; the fiducial region contained about half of the counts of the bin. The ϕ acceptance for the bin was defined as the ϕ acceptance of the fiducial region times the ratio of total bin counts to counts in the fiducial region. This method of calculating the ϕ acceptance increases the statistical error on the differential cross section. For most spectrometer settings the ϕ acceptance varied rather slowly and smoothly, except for statistical fluctuations, from bin to bin. The ϕ acceptance finally used was the smoothed value determined by fitting a quadratic polynomial to θ-vs-ϕ acceptance.

C. Differential cross sections

The differential cross section for each run was calculated in the c.m. frame of reference using

$$\frac{d\sigma}{d\Omega^*} = \frac{n}{\Delta\Omega^* NRM\epsilon} ,$$

where n = number of counts in each c.m. angle bin for the run, $\Delta\Omega^*$ = solid angle in the c.m. system for the bin, N = nominal number of target protons/cm^2 traversed by the beam, R = number of incident protons for each beam monitor count, M = number of beam monitor counts gated by the live time, and ϵ = product of the efficiencies and other corrections applied to the data. The errors in these quantities were added in quadrature to get the final error in $d\sigma/d\Omega^*$. For runs whose spectrometer settings overlapped, the final cross sections were found by weighted averages. The rest of this section is devoted to a discussion of these quantities, including estimations of their errors.

The counts and solid angle per c.m. bin have already been discussed. The error in n was taken to be statistical: $\sqrt{n}$. The fractional error in $\Delta\Omega^*$ was estimated to be $1/(2\sqrt{n})$.

The number of protons/cm^2 in the target was calculated from

$$N = \rho l N_0/m ,$$

where ρ is the density of liquid hydrogen (nominally about 0.071 g/cm^3 and measured for each run to 1%), l is the nominal target length, N_0 is Avogadro's number, and m is the mass of one mole of hydrogen. Because of the curved ends of the target, it was necessary to apply a length correction which was absorbed in ϵ. (See discussion below.)

The error in R was 1.4% from the beam calibration. As a check on the beam calibration, periodic runs of pp elastic scattering near 90° (in the c.m. frame) were taken. Our measured pp elastic cross sections agree within errors with published data.[18]

The number of beam monitor counts during a data run and the effect of system live time were both contained in M. This quantity was found by counting beam monitor events only during times when the system was live and capable of accepting events. Due to the arrangement of the electronics, what we called the multiwire-proportional-chamber efficiency was already included in the dead-time circuitry; hence, no separate adjustment for chamber efficiency was needed. This is seen as follows: The chamber electronics allowed only one particle at a time to fire a chamber and kept the chamber dead a few hundred nsec after it did fire. Because of the high singles rate in each chamber (several times 10^5/sec) each chamber was dead generally about 5% to 10% of the time, with a resulting apparent efficiency of 90% to 95%. The logic required at least two out of three chambers in a view to fire for all four views for an event to be accepted, but the live-time circuit turned the system off anyway if two or more cham-

bers in any view were dead simultaneously. Thus the apparent chamber inefficiencies were absorbed in the dead-time correction. The actual chamber efficiency was better than 99% as determined in tests in which the dead time from multiparticle events was measured.

There were several efficiencies and adjustments that were applied to the cross-section calculations. All of these were included in ϵ. These corrections were as follows.

1. Time-of-flight counter efficiency

Events were lost due to inefficiencies in the deuteron TOF counters. With two separate TOF measurements (one used scintillators 1 and 3 while the other used 2 and 4) an event was accepted only if at least one TOF fired. Letting e_i be the four scintillator efficiencies, the individual TOF inefficiencies were $\bar{e}_{13} = 1 - e_1 e_3$ and $\bar{e}_{24} = 1 - e_2 e_4$; thus the total TOF efficiency was calculated from $e(\mathrm{TOF}) = 1 - \bar{e}_{13}\bar{e}_{24}$. The numbers $\bar{e}_{13}$ and $\bar{e}_{24}$ were found by counting the events missed by the corresponding TOF counters. The total TOF efficiency was generally about 0.995 with a 0.5% error.

2. Pion counter efficiency

Under normal operating conditions the scintillator in the pion arm was required to fire for an acceptable event. In order to measure its efficiency, runs (usually on pp elastic scattering) were periodically taken in which the pion counter was not required in the logic but counts were recorded. If the running conditions were sufficiently stringent, such that the events accepted still corresponded to pp elastic scattering, then the ratio of pion nulls to accepted events gave the pion counter inefficiency. The pion scintillator efficiency, determined in this fashion, was 0.982 with an error of 2%.

3. Pion decay correction

A correction allowing for in-flight pion decay was applied to the data. This correction was $e(\mathrm{decay}) = \exp(-t/\gamma\tau)$, where t was the TOF between target and pion scintillator and $\gamma\tau$ the pion lifetime in the laboratory. For simplicity, the average pion momentum for the spectrometer arm setting was used for t and γ. The correction varied between 0.931 and 0.978, with an estimated error of 0.5%. But could muons from pion decay simulate good events? Not likely! The decay would have to take place very close to the end of the trajectory and the muon would have to come very forward. It was estimated that, over the whole trajectory, only 10% to 15% of the muons survived the proportional-chamber look-up logic; since only about 5% of the pions decayed, only 0.8% more events were accepted by the hardware than should have been. Of these, most were probably rejected by the software cuts in the off-line analysis.

4. Linearity correction

The linearity test of the orbits through the wire chambers has already been described. Since the linearity efficiency was measured by the on-line software for each view, the total linearity correction was the product of the four linearity efficiencies. It was ususally about 0.95 with negligible error.

5. Nuclear absorption

In addition to multiple Coulomb scattering, which broadened the resolution, the three particles of interest (proton, deuteron, and pion) also occasionally underwent strong interactions with the material of the apparatus, with the result that not all particles were detected. The transmission of each type of particle through the apparatus was calculated from

$$T_x = \exp\left[-\sum_i \sigma_{xi}(p_x)\, N_i\, L_i\right],$$

where x stands for proton, deuteron, or pion; $\sigma_{xi}(p_x)$ is the total cross section of particle x at momentum p_x for material i: N_i is the number of type-i atoms per unit volume; and L_i is the total length of material i. Since the cross sections are not generally well known, we approximated them by

$$\sigma_{xi}(p_x) \simeq \sigma_{xN}(p_x) A_i^{2/3},$$

where A_i is the atomic number of type-i atoms and $\sigma_{xN}(p_x)$ is the x-nucleon cross section. These are fairly well known.

The correction for the absorption in the beam line was 1.01, nearly independent of the beam momentum. It was greater than unity since the activation of the polystyrene sample was less than it should have been due to the absorption in the target and other material between the target and sample. The absorption correction in the deuteron arm was typically 0.94, depending on the deuteron momentum; for the pion arm it was usually about 0.99. The over-all error in each nuclear absorption correction was 0.6%, which included uncertainties in the amount of material as well as a 10% estimated uncertainty in the cross section.

6. Target-length correction

The two liquid hydrogen targets used in the experiment had curved ends; in general, beam particles did not traverse the full nominal length. Assuming a triangular distribution across the beam

TABLE I. Differential cross sections $d\sigma/d\Omega^*$ (μb/sr) from 3.0 to 5.0 GeV/c.

c.m. angle (degrees)	Momentum (GeV/c)															
	3.000		3.200		3.426		3.651		3.825		4.000		4.200		5.046	
1.0	9.92	0.54	15.8	1.1	14.9	1.2			13.5	1.2	9.48	1.00				
2.5											10.3	1.1				
3.0	9.84	0.44	15.62	0.99	15.4	1.2	13.66	0.67	15.2	1.1			8.27	0.77		
4.5					14.5	1.3										
5.0			15.8	1.1			13.30	0.70	12.8	1.0			9.00	0.78		
7.0			15.1	1.0			12.77	0.75					8.92	0.78	2.73	0.33
8.0									11.49	0.79						
8.5			14.1	1.0									7.64	0.61		
11.5									10.59	0.84			6.96	0.84		
12.5							8.5	1.3	9.29	0.76			7.09	0.84		
13.5							8.4	1.2	8.70	0.71			7.05	0.83	1.79	0.33
14.5			10.63	0.70			8.9	1.2	8.49	0.70			5.83	0.74	1.47	0.29
15.5			10.78	0.70			8.6	1.2	8.41	0.69	6.12	0.66	5.93	0.75	1.51	0.29
16.5	7.51	0.74	9.70	0.64	7.2	1.1	7.3	1.0	7.53	0.63	6.05	0.65	4.90	0.67	1.32	0.27
17.5	6.97	0.69	7.81	0.54	7.6	1.2	7.46	0.71	7.18	0.61	5.11	0.56	3.94	0.60	1.46	0.28
18.5	5.30	0.57	7.91	0.54	7.6	1.2	7.49	0.90	6.69	0.52	4.84	0.53	3.75	0.59	1.65	0.30
19.5	6.59	0.66	8.72	0.58	5.51	0.97	5.77	0.75	6.06	0.48	4.46	0.50	3.69	0.58	1.11	0.24
20.5	7.72	0.73	7.74	0.53	7.9	1.2	7.30	0.85	5.99	0.47	4.27	0.48			0.89	0.21
21.5	6.74	0.66	6.93	0.41	5.30	0.94	7.06	0.82	5.04	0.41					1.26	0.26
22.5	6.43	0.64	6.87	0.40	6.2	1.0	5.53	0.70	4.72	0.39					0.87	0.21
23.5	5.90	0.59	6.25	0.37	5.57	0.96	4.84	0.63	4.82	0.39			2.78	0.22		
24.5	6.49	0.64	6.05	0.36	5.67	0.96	4.83	0.63	3.95	0.34			2.64	0.22	0.87	0.20
25.5	5.84	0.59	6.30	0.54	6.13	1.00	4.59	0.60	3.93	0.33			2.38	0.20	0.717	0.093
26.5	6.37	0.63	6.02	0.52			4.13	0.56	3.87	0.33	3.35	0.41	2.30	0.19	0.86	0.10
27.5			5.91	0.51			3.71	0.53	3.61	0.31	2.96	0.37	2.22	0.19	0.638	0.085
28.5	7.08	0.91	6.20	0.39			3.60	0.30	3.55	0.23	3.07	0.38	1.86	0.17	0.703	0.089
29.5	6.22	0.81	5.60	0.36			3.81	0.32	3.11	0.21	2.76	0.35	2.02	0.17	0.552	0.076
30.5	6.19	0.80	5.68	0.36	5.30	0.63	3.31	0.29	2.90	0.20	2.83	0.22	1.73	0.15	0.436	0.066
31.5	6.13	0.79	5.31	0.35	4.13	0.52	2.82	0.30	2.93	0.26	2.61	0.21	1.73	0.15	0.411	0.063
32.5	6.38	0.82	5.25	0.44	3.90	0.50	3.40	0.34	2.53	0.23	2.35	0.19	1.85	0.11	0.407	0.062
33.5	5.71	0.74	5.03	0.42	4.04	0.50	2.98	0.31	2.85	0.25	2.16	0.18	1.68	0.11	0.403	0.061
34.5	5.56	0.72	5.22	0.37	3.89	0.49	2.43	0.27	2.42	0.22	2.16	0.18	1.60	0.10	0.279	0.050
35.5	5.30	0.69	4.63	0.34	4.24	0.52	3.08	0.31	2.31	0.21	1.78	0.16	1.493	0.097	0.353	0.056
36.5	5.06	0.66	4.67	0.27	3.61	0.46	2.37	0.26	2.37	0.21	1.86	0.19	1.407	0.093	0.362	0.057
37.5	4.56	0.60	4.59	0.27	3.43	0.26	2.29	0.25	2.14	0.15	1.87	0.19	1.45	0.12	0.308	0.052
38.5	4.54	0.60	4.13	0.25	3.28	0.25	2.04	0.23	2.02	0.14	1.78	0.19	1.26	0.11	0.391	0.068
39.5			4.55	0.32	3.10	0.24	2.31	0.25	1.91	0.17			1.32	0.11	0.334	0.062
40.5			4.05	0.29	3.20	0.25			1.78	0.16			1.147	0.100	0.312	0.060
41.5			3.84	0.28	3.04	0.24			1.71	0.16			1.099	0.096	0.264	0.055
42.5	4.21	0.59	3.76	0.27	3.15	0.28			1.80	0.16			0.988	0.089	0.242	0.049
43.5	4.23	0.33	3.81	0.27	2.73	0.25	2.24	0.21	1.76	0.12			0.978	0.088	0.192	0.043
44.5	4.71	0.36	3.44	0.29	2.59	0.17	1.97	0.19	1.70	0.12			0.838	0.079	0.142	0.036
45.5	4.34	0.33	3.35	0.28	2.62	0.17	2.01	0.19	1.55	0.11	1.215	0.084	0.815	0.056	0.114	0.032
46.5	4.08	0.32	3.06	0.26	2.49	0.17	1.91	0.18	1.55	0.11	1.083	0.077	0.795	0.070	0.093	0.029
47.5	3.98	0.31	3.56	0.23	2.42	0.16	1.76	0.17	1.383	0.099	1.055	0.076	0.866	0.074	0.112	0.032
48.5	3.83	0.30	3.33	0.21	2.22	0.15	1.54	0.15	1.345	0.097	1.091	0.077	0.767	0.068	0.098	0.029
49.5	3.34	0.48	3.23	0.21	2.22	0.15	1.80	0.17	1.31	0.13	0.979	0.071	0.707	0.064	0.150	0.037
50.5	2.96	0.43	3.04	0.20	2.07	0.14	1.43	0.14	1.32	0.13	0.972	0.071	0.714	0.065	0.142	0.036
51.5			2.74	0.18	2.00	0.18	1.61	0.16	1.16	0.11	0.929	0.068	0.658	0.061	0.097	0.029
52.5	3.34	0.47	2.62	0.17	1.95	0.14	1.39	0.11	1.10	0.11	0.899	0.066	0.592	0.057	0.135	0.034
53.5	3.08	0.43	2.54	0.17	1.80	0.13	1.30	0.11	0.919	0.097	0.853	0.075	0.648	0.060	0.122	0.032
54.5	3.06	0.43	2.51	0.17	1.78	0.11	1.24	0.10	0.98	0.10	0.821	0.073	0.635	0.059	0.051	0.021
55.5	3.16	0.44	2.28	0.15	1.84	0.12	1.21	0.10	0.955	0.099	0.703	0.066	0.627	0.058	0.058	0.022
56.5	2.82	0.21	2.44	0.16	1.56	0.10	1.04	0.14	0.99	0.10	0.678	0.064	0.520	0.040	0.083	0.027
57.5	2.65	0.18	2.07	0.14	1.66	0.11	1.27	0.16	0.879	0.093	0.672	0.063	0.527	0.040	0.109	0.031
58.5	2.62	0.18			1.53	0.12	1.07	0.15	0.859	0.091	0.693	0.081	0.484	0.038		
59.5	2.23	0.16	1.95	0.15	1.38	0.11	1.16	0.15	0.762	0.083	0.590	0.071	0.512	0.057	0.109	0.024
60.5	2.24	0.16	1.85	0.15	1.27	0.11	1.20	0.15	0.868	0.090	0.625	0.074	0.468	0.053	0.114	0.024
61.5	2.17	0.16	1.69	0.14	1.34	0.11	0.888	0.078	0.674	0.076	0.663	0.077	0.474	0.054	0.092	0.021
62.5	2.24	0.17	1.68	0.13	1.23	0.10	0.930	0.080	0.758	0.082	0.603	0.071	0.498	0.055	0.087	0.021
63.5	1.90	0.15	1.49	0.12	1.08	0.12	0.756	0.068	0.722	0.080	0.534	0.065	0.455	0.052	0.083	0.020
64.5	1.70	0.13	1.42	0.12	1.06	0.12	0.926	0.078	0.590	0.070	0.452	0.057	0.460	0.052	0.100	0.022

TABLE I *(Continued)*

c.m. angle (degrees)	Momentum (GeV/c) 3.000		3.200		3.426		3.651		3.825		4.000		4.200		5.046	
65.5	1.45	0.12	1.36	0.11	0.95	0.11	0.728	0.066	0.646	0.074	0.490	0.060			0.082	0.020
66.5	1.51	0.12	1.24	0.11			0.688	0.075	0.601	0.071	0.458	0.057			0.096	0.022
67.5	1.41	0.12	1.084	0.095			0.647	0.072	0.576	0.069	0.420	0.054			0.106	0.023
68.5	1.18	0.10	1.061	0.093			0.698	0.075	0.538	0.067	0.415	0.053			0.096	0.022
69.5	1.23	0.11	0.933	0.085	0.819	0.066	0.590	0.067			0.453	0.057	0.342	0.032	0.090	0.021
70.5			0.969	0.062	0.752	0.061	0.547	0.064	0.596	0.067			0.367	0.033	0.077	0.019
71.5			0.864	0.056	0.711	0.058	0.506	0.061	0.546	0.063			0.342	0.031	0.063	0.017
72.5	1.44	0.21	0.820	0.054	0.649	0.054	0.579	0.067	0.597	0.066			0.329	0.031	0.057	0.017
73.5	1.17	0.18	0.796	0.065	0.595	0.051			0.415	0.052	0.405	0.027	0.327	0.030	0.073	0.019
74.5	1.06	0.17	0.743	0.061	0.555	0.048			0.456	0.055	0.376	0.026	0.300	0.028		
75.5	1.03	0.16	0.660	0.055	0.537	0.047			0.419	0.052	0.371	0.025	0.267	0.026	0.066	0.017
76.5	0.82	0.13	0.622	0.053	0.548	0.041			0.355	0.047	0.337	0.024	0.242	0.024	0.074	0.018
77.5	0.94	0.15	0.568	0.049	0.472	0.036			0.350	0.046	0.319	0.023	0.244	0.025	0.105	0.022
78.5	0.81	0.13	0.499	0.045	0.438	0.034			0.373	0.048	0.305	0.022	0.210	0.022	0.063	0.017
79.5	0.71	0.12	0.425	0.040	0.427	0.034			0.313	0.043	0.269	0.020	0.229	0.024	0.047	0.014
80.5	0.63	0.11	0.466	0.042	0.378	0.051			0.331	0.045	0.250	0.019			0.056	0.016
81.5	0.62	0.11	0.437	0.041	0.382	0.051			0.283	0.027	0.243	0.019	0.240	0.039	0.035	0.012
82.5	0.556	0.098			0.289	0.043			0.260	0.032	0.261	0.020	0.293	0.043	0.041	0.013
83.5	0.579	0.086	0.369	0.038	0.285	0.026	0.344	0.061	0.234	0.030			0.208	0.035	0.039	0.013
84.5	0.598	0.089	0.361	0.037	0.248	0.020	0.309	0.056	0.273	0.033			0.246	0.036	0.056	0.016
85.5	0.605	0.067	0.374	0.038	0.289	0.022	0.286	0.036	0.231	0.030	0.245	0.021	0.201	0.034	0.037	0.013
86.5	0.610	0.068	0.361	0.037	0.304	0.023	0.281	0.035	0.209	0.028	0.222	0.020	0.171	0.031	0.063	0.017
87.5	0.540	0.061	0.325	0.025	0.251	0.020	0.212	0.030	0.229	0.029	0.232	0.021	0.224	0.036	0.040	0.014
88.5	0.482	0.056	0.319	0.025	0.253	0.020	0.271	0.034	0.223	0.029	0.188	0.018	0.198	0.024	0.031	0.012
89.5	0.551	0.062	0.313	0.024	0.285	0.024	0.248	0.032	0.223	0.021	0.212	0.019	0.198	0.024	0.033	0.013

as indicated by the beam profile monitors, the length correction for the larger target was estimated at 0.97 with a 3% error. For the smaller target the correction was larger. Whenever possible, runs with the smaller target were normalized to the larger-target runs by using *pp* elastic scattering data taken with both targets. This generally involved a 10% to 15% correction with a 5% error. For the 5-GeV/*c* data, where the larger target was not used, the length correction was taken as 0.96 with a 5% error.

7. *Dead-time correction*

It was found that our monitoring of the dead time did not account for all rate-dependent effects and that a correction had to be applied to our cross section. A calibration of the effect has been done with runs of *pp* elastic scattering at various intensities. At a rate corresponding to 20% dead time, this correction amounted to $(5 \pm 2.5)\%$.

In summary, all these systematic errors were added in quadrature, giving 4.5% for the large target and 6% for the small target.

IV. RESULTS AND DISCUSSIONS

We have measured the differential cross section at eight values of incident proton momentum: 3.000, 3.200, 3.426, 3.651, 3.825, 4.000, 4.200, and 5.046 GeV/*c*. These data are presented in Table I. In the table we list the cross section in 1° c.m. bins with their errors. The bins are nearly continuous over the entire range from 0° to 90°. Some small regions of the angular distribution were not accessible with this apparatus for kinematic reasons.

The errors are compounded from the statistical error based on the number of events collected in each bin, the uncertainty in the esitmation of the solid-angle acceptance, and systematic errors of measurement as described above. All errors are compounded by taking the square root of the sum of their squares as if they were all random and independent. This condition is reasonably well satisfied in stating the error for each 1° bin as given. However, in summing over a set of adjacent bins, only the statistical part of the relative error will be reduced by the augmented number of events included, the systematic part, which amounts to about 6%, is not reduced for such combinations. Thus, the total cross section, obtained by integrating over the full angular range, which would have a statistical contribution of less than 0.4% for most of our runs, must be assigned an error of about 6% because of the systematic uncertainties of our measurement.

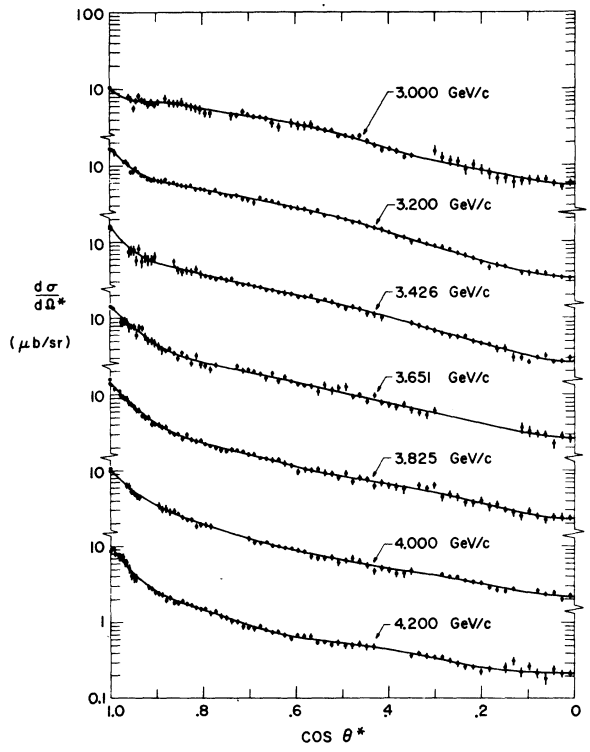

FIG. 5. The differential cross sections for the reaction $pp \to d\pi^+$ in the c.m. system at seven of the eight incident momenta studied in this experiment. The solid lines are even-order Legendre polynomial fits to the data.

The general trend of the data can be seen in Fig. 5. In this figure the solid lines are Legendre polynomial fits to the data. The 5-GeV/c data has been omitted from this just to emphasize the greater detail with which the region between 3.0 and 4.2 GeV/c was studied.

Using Legendre fits we display in Fig. 6 the cross sections from this and other experiments

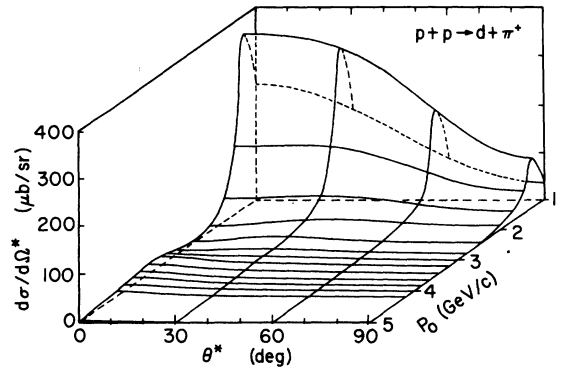

FIG. 6. Even-order Legendre polynomial fits to the $pp \to d\pi^+$ data from Ref. 2, Ref. 7, and the present experiment between 1 and 5 GeV/c incident momentum.

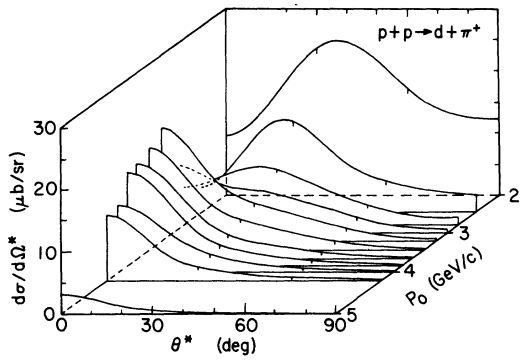

FIG. 7. The same data as in Fig. 6 between 2 and 5 GeV/c. This reduced range in incident momentum is shown to emphasize the behavior near 0° in the c.m. system.

between 1 and 5 GeV/c. In Fig. 7 we show the data between 2 and 5 GeV/c in order to emphasize the 0° structure between 3.0 and 4.0 GeV/c. This shows that the enhancement in the forward direction near 3.6 GeV/c vanishes rapidly for larger values of the production angle. Thus the influence of the $\Delta(1950)$ is evident only in the forward direction. In contrast, the effect of the $\Delta(1236)$ resonance near 1.25 GeV/c is prominent over whole angular ranges.

The total cross sections, obtained by integrating over the angular distribution using the fitted values of the coefficients of the Legendre polynomials ($\sigma_T = 4\pi b_0$), are shown in Fig. 8 and listed in Table II. For comparison we also show the pp elastic, $pn\pi^+$, $pp\pi^0$, and total cross sections.[19] We have included the low-energy data from Heinz *et al.*[7] and the high-energy data of Amaldi *et al.*[20] and Allaby *et al.*[21] The high-energy data cover only a narrow angular range near 0°. Therefore, the total cross sections were found by integrating fits of the form $d\sigma/d\Omega^* = Ae^{-P_\perp/b}$ to their angular-distribution measurements. It is seen that the $pp \to d\pi^+$ cross section drops steeply. The slope is $\sim P_0^{-4}$, as is commonly found in nucleon exchange processes.[22] In addition, we see that there is a shoulder at 3.0 GeV/c corresponding to the excitation of the $\Delta(1950)$. As will be discussed later, it is mainly the forward cross section which shows strong peaking. This behavior carries over into the total cross section, giving evidence that the $\Delta(1950)$ plays an important role in this reaction, as predicted by Chahoud et al.[4] and Yao.[5]

We have fitted our data by a least-squares procedure to a series of even-order Legendre polynomials:

$$\frac{d\sigma}{d\Omega^*} = \sum_{l=0}^{n} b_{2l} P_{2l}(\cos\theta) \ .$$

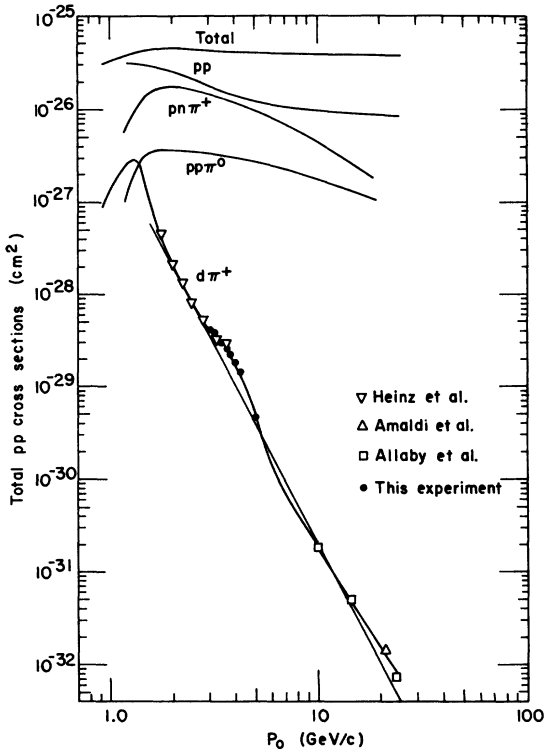

FIG. 8. The total cross sections of the various pp channels as a function of incident momentum. The pp elastic, $pn\pi^+$, and $pp\pi^0$ data are from Ref. 19. The data points of the $d\pi^+$ channel for the present experiment were found by multiplying the fitted Legendre polynomial coefficient b_0 by 4π. A curve of the form $\sigma_T(pp \to d\pi^+) \sim P_0^{-C}$ was fitted to the data including previously published work (Refs. 7, 20, 21).

A good fit was obtained ($\chi^2/N \sim 1$ for $N = 50$ to 70 degrees of freedom) with $n = 7$. The parameters of these fits with their errors are given in Table III. The coefficients b_{12} and b_{14} have low significance and are included only for completeness. The variation of the parameters with momentum is shown in Fig. 9, in which the coefficients at each momentum are normalized to b_0. We have also included the low-momentum data of Richard-Serre *et al.*[2] from 1.18 to 1.48 GeV/c and those of Heinz *et al.*[7] from 1.7 to 2.8 GeV/c. The solid lines are hand-drawn through the points to guide the eye. In the low-energy region b_2/b_0 goes through a minimum at 2.0 GeV/c, while b_4/b_0 and b_6/b_0 are negative and peak respectively at 2.0 and 2.5 GeV/c. It is of interest to note how smooth the transition is from one experiment to the next, showing the quality of the data. Also it is interesting that the b_6 and higher coefficients all become close to zero near 3.0 GeV/c.

TABLE II. Total cross sections.

P_0 (GeV/c)	σ (μb)	Error (μb)
3.000	36.9	2.2
3.200	35.1	2.1
3.426	28.3	1.7
3.651	23.2	1.4
3.825	20.8	1.2
4.000	16.5	1.0
4.200	13.2	0.8
5.046	3.4	0.2

Above 3.0 GeV/c all coefficients rise rapidly with increasing momentum, implying that new angular momentum channels are becoming important. However, the fact that none of the coefficients has a significant structure makes it impossible to pick out a particular angular momentum component of the reaction corresponding to the $\Delta(1950)$ resonance. The 4.0-GeV/c points are all low; however, we believe this to be a slight anomaly in the data.

In Fig. 10 we show the momentum variation of the cross section at a series of fixed angles. This figure emphasizes the earlier point that there is an enhancement only in the forward direction over about the first 20°. Beyond that angle the cross section falls relatively smoothly, and close to 90° it even appears to be reduced in the resonance region. Since the enhancement assigned to the

TABLE III. Legendre polynomial coefficients.

P_0 (GeV/c)	b_0 (μb/sr)	b_2 (μb/sr)	b_4 (μb/sr)	b_6 (μb/sr)	b_8 (μb/sr)	b_{10} (μb/sr)	b_{12} (μb/sr)	b_{14} (μb/sr)	χ^2/N
3.000	2.93 ± 0.04	4.95 ± 0.11	0.06 ± 0.14	0.13 ± 0.19	0.58 ± 0.18	0.36 ± 0.18	0.49 ± 0.21	0.49 ± 0.18	0.6
3.200	2.80 ± 0.02	5.93 ± 0.08	2.13 ± 0.11	1.97 ± 0.13	1.70 ± 0.14	1.08 ± 0.14	0.67 ± 0.15	0.25 ± 0.11	0.5
3.426	2.25 ± 0.04	5.06 ± 0.16	2.42 ± 0.19	1.99 ± 0.20	1.48 ± 0.21	1.07 ± 0.21	0.65 ± 0.20	0.22 ± 0.13	0.5
3.651	1.85 ± 0.03	4.47 ± 0.10	2.94 ± 0.12	2.32 ± 0.12	1.45 ± 0.13	0.65 ± 0.15	0.14 ± 0.15	0.06 ± 0.14	0.7
3.825	1.66 ± 0.02	4.18 ± 0.07	3.05 ± 0.09	2.34 ± 0.11	1.46 ± 0.12	0.87 ± 0.12	0.23 ± 0.12	0.01 ± 0.08	0.4
4.000	1.31 ± 0.02	3.23 ± 0.10	2.21 ± 0.13	1.42 ± 0.15	0.77 ± 0.16	0.49 ± 0.16	0.20 ± 0.13	0.08 ± 0.08	0.5
4.200	1.05 ± 0.02	2.64 ± 0.06	2.11 ± 0.08	1.61 ± 0.09	1.03 ± 0.09	0.73 ± 0.09	0.40 ± 0.09	0.06 ± 0.06	0.5
5.046	0.27 ± 0.01	0.79 ± 0.04	0.76 ± 0.06	0.53 ± 0.07	0.26 ± 0.07	0.20 ± 0.06	0.10 ± 0.06	0.01 ± 0.03	0.8

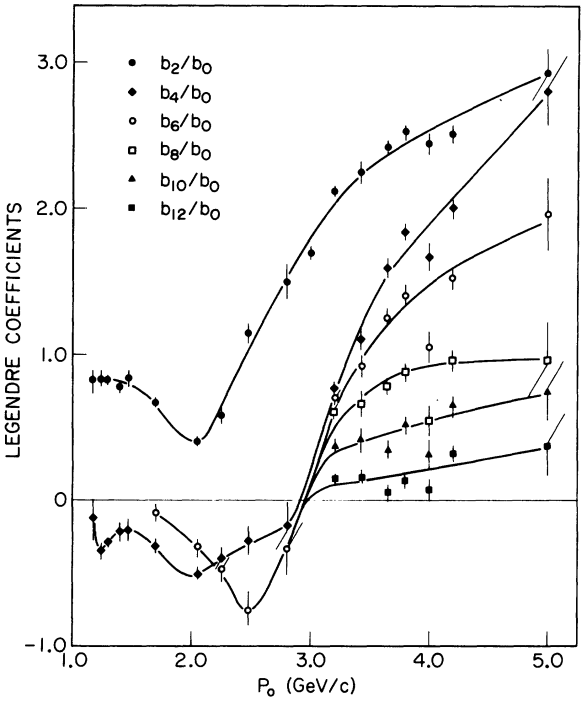

FIG. 9. The variation of the Legendre polynomial coefficients with incident momentum. The coefficients are normalized to b_0. The smooth curves are freehand lines drawn for clarity. The data of Ref. 2 were used between 1.18 and 1.48 GeV/c. The data of Ref. 7 were used between 1.7 and 2.8 GeV/c.

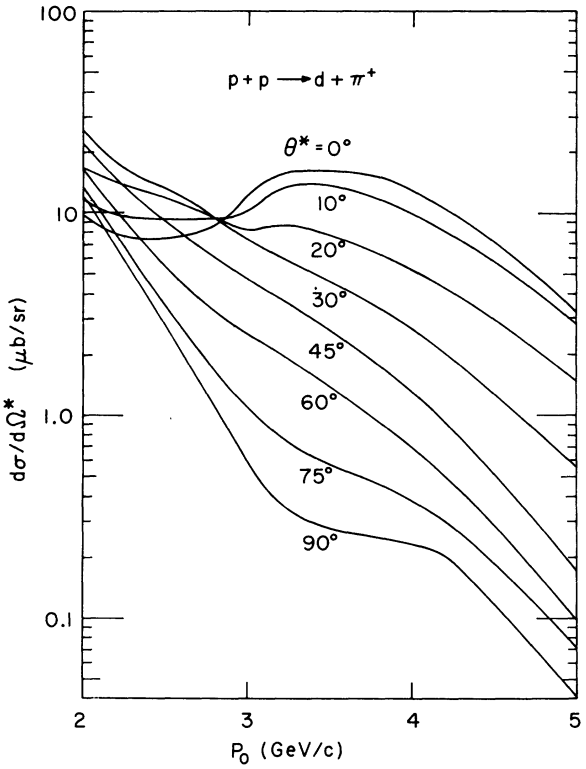

FIG. 10. The differential cross sections of the $pp \rightarrow d\pi^+$ reaction as a function of incident momentum between 2 and 5 GeV/c for various c.m. angles.

$\Delta(1950)$ markedly affects only the forward cross section, the angular distribution at the higher angles is likely to be dominated by other processes.

At high energies the differential cross sections of Amaldi *et al.*[20] and Allaby *et al.*,[21] plotted as a function of the transverse momentum, show a single slope over the limited angular ranges of their data. The same general slope also fits our data at much lower energies. However, there are significant deviations near 0° and near 90°.

Barry[9] has given a prescription for calculating the differential cross section based on the one-pion-exchange (OPE) model, Fig. 11(a), and the calculation of Yao.[5] Sundaresan and Watson[10] have used this prescription and compared the calculation with our results. In general the agreement is poor, although some features are reproduced. One concludes that the OPE model does not give a good representation of our more complete data at these energies, presumably because of the inadequacies of the model in handling the behavior of the $pn\pi^+$ vertex far from the mass shell.

Other models have been tried on earlier data. [See, for instance, Refs. 7, 23, and 24 for one-nucleon exchange, Fig. 11(b).] The comparison with earlier data shows that no good fit has been possible. Reggeized one-nucleon exchange has been tried at the higher energies with limited success by Lee[25] and Barger and Michael.[26] Regge behavior for reaction (1), however, as discussed by Dubal,[27] shows up only above 10 GeV/c and therefore is of no help in understanding the data of this experiment.

In an early paper on the nucleon pickup process Chew and Goldberger[28] introduced the variable $\Delta = |p^* - \frac{1}{2}d^*|$, where p^* and d^* are the three-momenta of the incident particle and the deuteron,

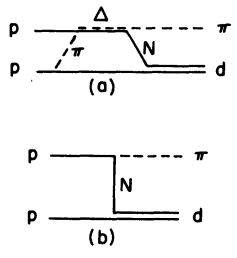

FIG. 11. (a) One-pion-exchange diagram for $pp \rightarrow d\pi^+$; (b) one-nucleon-exchange diagram for $pp \rightarrow d\pi^+$.

respectively, in the c.m. system. This is just a measure of the relative momentum of the two nucleons in the deuteron. The variable has been used by Kerman and Kisslinger[11] in the case of pd backward elastic scattering, and has been found to remove the s dependence of the differential cross section. In Fig. 12 the data of the current experiment are plotted against this variable (we chose that nucleon which gives the smaller Δ), where for clarity we have included only three of our momenta, spanning the interval from 3.0 to 4.2 GeV/c. The curves for intermediate momenta cluster close to the curves shown and give the effect of a cross section that varies over the range of Δ with relatively little s dependence. There are deviations at small values of Δ due presumably to the effect of the $\Delta(1950)$ resonance. This parametrization is less impressive as the available data both below and above our range are included.

A given value of Δ fixes the role of the deuteron wave function in determining the cross section. Thus variations in the cross section at fixed Δ reflect the influence of other factors which enter into the process, e.g., the $pn\pi^+$ vertex.

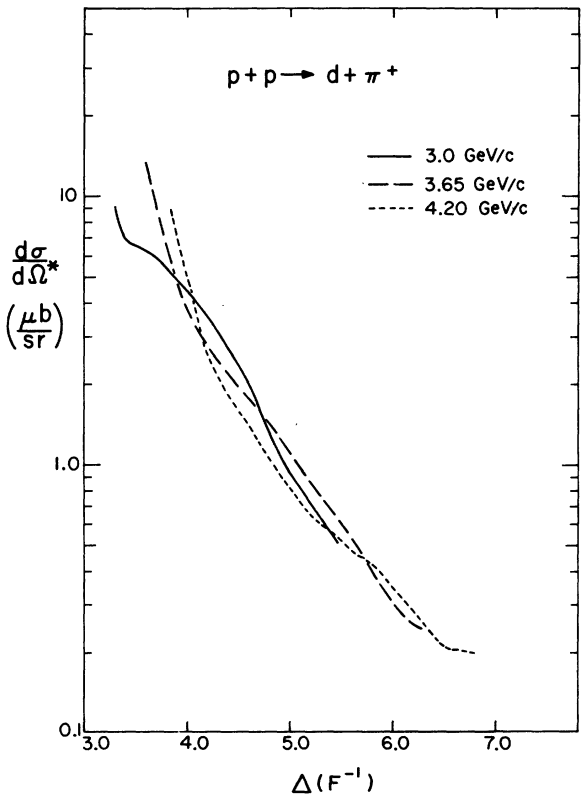

FIG. 12 The $pp \to d\pi^+$ differential cross section as a function of the momentum parameter $\Delta = |p^* - \frac{1}{2}d^*|$ for three incident momenta.

V. CONCLUSIONS

We have made extensive measurements of the $pp \to d\pi^+$ differential cross section over a range of incident proton momenta from 3.0 to 5.0 GeV/c. The measured cross sections exhibit a strong dependence on momentum transfer and energy. At 3.83 GeV/c, for example, the differential cross section falls from 14 μb/sr in the forward direction to 0.2 μb/sr at 90° (c.m.). The total cross section falls from 37 μb at 3 GeV/c to 3.4 μb at 5 GeV/c, much faster than in the corresponding reaction $pp \to pn\pi^+$ in which the proton and neutron emerge unbound.

The data show that the previously observed enhancement in the forward cross section between 3 and 4 GeV/c is an effect which damps out quickly as the production angle departs from 0°, in contrast to the well-known enhancement at 1.35 GeV/c, which is evident at all angles. The coefficients of even-order Legendre-polynomial fits to the data increase smoothly with momentum. There is no evidence that any one angular momentum state plays a dominant role in the process between 3 and 5 GeV/c. The OPE model was found not to give a good description of our data over the more complete angular range covered in this work, presumably because of the inadequacies in accounting for off-mass-shell effects.

A single parameter Δ which measures the relative momentum of the proton and neutron in the deuteron suffices to determine the behavior of the cross section over most of the range of our data, relatively independent of the incident momentum. This emphasizes the importance of the deuteron form factor in the process.

ACKNOWLEDGMENTS

We wish to thank C. Halliwell, T. K. Ohska, and J. Walters for their assistance in the running of the experiment. M. K. Sundaresan and P. J. S. Watson were most helpful in interpreting the data. B. C. Smith's work in programming the computer with help from R. P. Singh in the later stages was invaluable. The contributions of R. L. Armstrong, G. S. Black, R. R. Gabriel, J. P. Legault, R. Ryan, R. Sancton, and M. Wenger in the design, construction, and maintenance of the apparatus were essential to the success of the experiment. T. A. Nunamaker and D. Bernstein, with help from K. A. Klare, designed and constructed the electronic circuitry for the proportional chambers. A. Smith and J. McCaslin carried out the beam calibrations during the entire course of the experiment. D. Hunt and the Berkeley hydrogen target group de-

signed, manufactured, and maintained the hydrogen target for us. R. Sah designed the beam and calculated its properties. J. Forst and the Berkeley magnet test group measured the analyzing magnet. In addition, we wish to thank the Bevatron operations staff for their care and efforts in providing us with the beam. Finally we wish to thank the Lawrence Berkeley Laboratory for their over-all cooperation in carrying out this experiment.

---

*Research supported by the National Science Foundation, the U. S. Atomic Energy Commission, and the National Research Council of Canada. Submitted by D. A. Larson to the Department of Physics, The University of Chicago, in partial fulfillment of the requirements for the Ph.D. degree.

†Present address: Cornell University, Ithaca, New York 14850.

‡Present address: Swiss Institute for Nuclear Research, 5234 Villigen, Switzerland.

§Also at Carleton University, Ottawa, Canada.

‖Formerly at Carleton University, Ottawa, Canada.

**Present address: Carnegie-Mellon University, Pittsburgh, Pennsylvania 15213.

[1]H. L. Anderson, M. S. Dixit, H. J. Evans, K. A. Klare, D. A. Larson, M. V. Sherbrook, R. L. Martin, D. Kessler, D. E. Nagle, H. A. Thiessen, C. K. Hargrove, E. P. Hincks, and S. Fukui, Phys. Rev. D 3, 1536 (1971).

[2]M. G. Mescheryakov, B. S. Neganov, N. P. Bogachev, and V. M. Sidorov, Dokl. Akad. Nauk SSSR 100 (4), 674 (1955) [AERE Lib/trans. 552]; M. G. Mescheryakov, and B. S. Neganov, *ibid.* 100 (4), 677 (1955) [AERE Lib/trans 551]; T. H. Fields, J. G. Fox, J. A. Kane, R. A. Stallwood, and R. B. Sutton, Phys. Rev. 109, 1704 (1958); B. S. Neganov, and L. B. Parfenov, Zh. Eksp. Teor. Fiz. 34, 767 (1958) [Sov. Phys.—JETP 7, 528 (1958)]; C. Richard-Serre, W. Hirt, D. F. Measday, E. G. Michaelis, M. J. M. Saltmarsh, and P. Skarek, Nucl. Phys. B20, 413 (1970); C. L. Dolnick, *ibid.* B22, 461 (1970).

[3]S. Mandelstam, Proc. R. Soc. Lond. A244, 491 (1958).

[4]J. Chahoud, G. Russo, and F. Selleri, Phys. Rev. Lett. 11, 506 (1963).

[5]T. Yao, Phys. Rev. 134, B454 (1964).

[6]L. Dubal and D. J. Brown, Nucl. Phys. B32, 535 (1971).

[7]R. M. Heinz, O. E. Overseth, D. E. Pellett, and M. L. Perl, Phys. Rev. 167, 1232 (1968).

[8]D. Dekkers, B. Jordan, R. Mermod, C. C. Ting, G. Weber, T. R. Willits, K. Winter, X. De Bouard, and M. Vivargent, Phys. Lett. 11, 161 (1964).

[9]G. Barry, Ann. Phys. (N.Y.) 73, 482 (1972); N. S. Craigie, J. Körner, and I. O. Stamatescu, Phys. Lett. 42B, 404 (1972).

[10]M. K. Sundaresan and P. J. S. Watson, private communication.

[11]A. K. Kerman and L. S. Kisslinger, Phys. Rev. 180, 1483 (1969).

[12]J. McCaslin *et al.* (unpublished).

[13]C. K. Hargrove, J. P. Legault, L. Bird, H. Mes, R. Sancton, A. C. Thompson, and J. Walters (unpublished).

[14]G. Charpak, H. G. Fisher, C. R. Gruhn, A. Minter, F. Sauli, G. Puch, and G. Flugge, Nucl. Instrum. Methods 99, 279 (1972).

[15]T. A. Nunamaker, and D. Bernstein (unpublished).

[16]R. Gabriel (unpublished).

[17]A report describing this retrace method in detail is being prepared by R. J. McKee.

[18]The most comprehensive set of pp elastic data from 3 to 5 GeV/c is that of R. C. Kammerud, B. B. Brabson, R. R. Crittenden, R. M. Heinz, H. A. Neal, H. W. Park, and R. A. Sidwell, Phys. Rev. D 4, 1309 (1971). A report presenting our pp elastic data is in preparation.

[19]Particle Data Group, LBL Report No. UCRL-20 0000 *NN*, 1970 (unpublished), pp. 26 and 72.

[20]U. Amaldi, R. Biancastelli, C. Bosio, G. Matthiae, J. V. Allaby, A. N. Diddens, R. W. Dobinson, A. Klovning, J. Litt, L. S. Rochester, K. Schlupmann, and A. M. Wetherell, Nuovo Cimento Lett. 4, 121 (1972).

[21]J. V. Allaby, F. Binon, A. N. Diddens, P. Duteil, A. Klovning, R. Meunier, J. P. Peigneux, E. J. Sacharidis, K. Schlupmann, M. Spighel, J. P. Stroot, A. M. Thorndike, and A. M. Wetherell, Phys. Lett. 29B, 198 (1968).

[22]D. R. O. Morrison, Phys. Lett. 22, 528 (1966).

[23]D. J. Brown, Can. J. Phys. 47, 2001 (1969).

[24]F. Uchiyama-Campbell and R. R. Silbar, LASL Report No. LA-DC-10315, 1969 (unpublished).

[25]H. Lee, Phys. Rev. 174, 2130 (1968).

[26]V. Barger and C. Michael, Phys. Rev. Lett. 22, 1330 (1969).

[27]L. Dubal, Nuovo Cimento Lett. 5, 978 (1972).

[28]G. F. Chew and M. L. Goldberger, Phys. Rev. 77, 470 (1950).